NASA Technical Memorandum 102800

Extension of a Streamwise Upwind Algorithm to a Moving Grid System

Shigeru Obayashi
MCAT Institute, San Jose, California

Peter M. Goorjian and Guru P. Guruswamy
Ames Research Center, Moffett Field, California

April 1990

National Aeronautics and
Space Administration

Ames Research Center
Moffett Field, California 94035-1000

EXTENSION OF A STREAMWISE UPWIND ALGORITHM TO A MOVING GRID SYSTEM

Shigeru Obayashi,* Peter M. Goorjian, and Guru P. Guruswamy
Ames Research Center

SUMMARY

A new streamwise upwind algorithm has been derived to compute unsteady flow fields with the use of a moving-grid system. The temporally nonconservative LU-ADI (lower-upper-factored, alternating-direction-implicit) method has been applied for time-marching computations. A comparison of the temporally nonconservative method with a time-conservative implicit upwind method indicates that the solutions are insensitive to the conservative properties of the implicit solvers when practical time-steps are used. Using this new method, computations have been made for an oscillating wing at a transonic Mach number. The computed results confirm that the present upwind scheme captures the shock motion better than the central-difference scheme based on the Beam-Warming algorithm. The new upwind option of the code allows larger time-steps and thus is more efficient, even though it requires slightly more computational time per time-step than the central-difference option.

INTRODUCTION

A code, ENSAERO, is being developed at Ames using the Euler/Navier-Stokes equations for computing the unsteady aerodynamics and aeroelasticity of aircraft. The capability of the code has been demonstrated by computing vortical and transonic flows over flexible swept wings (refs. 1 and 2). The flow fields were calculated by a time-accurate, finite-difference scheme based on central differencing.

The purpose of this study is to enhance the algorithm capability of the present code. In this respect, the use of a new upwind scheme in comparison to the current central-difference (CD) scheme is investigated. The CD scheme requires an artificial dissipation to stabilize computations. Such artificial-dissipation models lead to more dissipative solutions than upwind schemes. In addition, the CD scheme is sensitive to the amount of dissipation and needs a specific dissipation coefficient for each case. On the other hand, upwind schemes do not require that any coefficient be specified.

Recently, a streamwise upwind algorithm has been developed and applied to treat steady-state problems of transonic flows over wings (ref. 3) and vortical flows over a delta wing (ref. 4) on fixed grids. The main feature of the streamwise method is the use of the local stream direction, flow velocity, and pressure gradient. The switching of flux evaluations always takes place at sonic values, where shock waves may exist. Therefore, this method follows the flow physics more closely than conventional upwind methods based

* MCAT Institute, San Jose, California.

on dimensional splitting. The computed results confirm the higher resolution of the present algorithm over the CD scheme, as well as over other upwind schemes.

In this paper, the streamwise upwind algorithm has been extended from fixed coordinates to moving coordinates for computing flows over moving components. The streamwise upwind scheme was applied to steady-state problems by using the lower-upper-factored, alternating-direction-implicit (LU-ADI) method in order to accelerate convergence (ref. 4). The same LU-ADI method, which is first-order accurate but nonconservative in time, is used in the present unsteady computations. In order to check the validity of the LU-ADI method for computations over moving grids, a conservative implicit version of the streamwise upwind scheme is also considered. The resulting algorithm has been implemented in the code as a finite-volume, upwind option, in addition to the previous CD option. The updated code has been successfully applied for computing unsteady transonic flows over an oscillating wing. The computed unsteady pressures are compared with the experimental data.

GOVERNING EQUATIONS

The nondimensionalized thin-layer Navier-Stokes equations used in this study can be written in conservation-law form in a generalized body-conforming curvilinear coordinate system (ξ, η, ζ) as follows:

$$\partial_\tau \hat{Q} + \partial_\xi \hat{E} + \partial_\eta \hat{F} + \partial_\zeta \hat{G} = \frac{1}{Re}\partial_\zeta \hat{G}^v \tag{1}$$

The Euler equations are obtained by setting the viscous flux vector $\hat{G}^v$ equal to zero. The vector of conserved quantities $\hat{Q}$ and the inviscid flux vectors $\hat{E}$, $\hat{F}$, and $\hat{G}$ are

$$\hat{Q} = \frac{1}{J}\begin{bmatrix} \rho \\ \rho u \\ \rho v \\ \rho w \\ e \end{bmatrix} \qquad \hat{E} = \frac{1}{J}\begin{bmatrix} \rho\hat{U} \\ \rho u\hat{U} + \xi_x p \\ \rho v\hat{U} + \xi_y p \\ \rho w\hat{U} + \xi_z p \\ \rho H\hat{U} - \xi_t p \end{bmatrix}$$

$$\hat{F} = \frac{1}{J}\begin{bmatrix} \rho\hat{V} \\ \rho u\hat{V} + \eta_x p \\ \rho v\hat{V} + \eta_y p \\ \rho w\hat{V} + \eta_z p \\ \rho H\hat{V} - \eta_t p \end{bmatrix} \qquad \hat{G} = \frac{1}{J}\begin{bmatrix} \rho\hat{W} \\ \rho u\hat{W} + \zeta_x p \\ \rho v\hat{W} + \zeta_y p \\ \rho w\hat{W} + \zeta_z p \\ \rho H\hat{W} - \zeta_t p \end{bmatrix}$$

where H is the total enthalpy, $H = (e + p)/\rho$, and the contravariant velocity components $\hat{U}$, $\hat{V}$, and $\hat{W}$ are defined as

$$\hat{U} = \xi_t + \xi_x u + \xi_y v + \xi_z w$$

$$\hat{V} = \eta_t + \eta_x u + \eta_y v + \eta_z w$$

$$\hat{W} = \zeta_t + \zeta_x u + \zeta_y v + \zeta_z w$$

The Cartesian velocity components u, v, and w are nondimensionalized by the free-stream speed of sound c_∞; the density ρ is nondimensionalized by the free-stream density ρ_∞; and the total energy per unit volume e is nondimensionalized by $\rho_\infty c_\infty^2$. The viscous flux vector $\widehat{G}^v$ is given by

$$\widehat{G}^v = \frac{1}{J}\begin{bmatrix} 0 \\ \mu m_1 u_\zeta + \frac{\mu}{3} m_2 \zeta_x \\ \mu m_1 v_\zeta + \frac{\mu}{3} m_2 \zeta_y \\ \mu m_1 w_\zeta + \frac{\mu}{3} m_2 \zeta_z \\ \mu m_1 m_3 + \frac{\mu}{3} m_2 (\zeta_x u + \zeta_y v + \zeta_z w) \end{bmatrix}$$

with

$$m_1 = \zeta_x^2 + \zeta_y^2 + \zeta_z^2$$

$$m_2 = \zeta_x u_\zeta + \zeta_y v_\zeta + \zeta_z w_\zeta$$

$$m_3 = \frac{1}{2}(u^2 + v^2 + w^2)_\zeta + \frac{1}{Pr\,(\gamma - 1)}(c^2)_\zeta$$

where Re is the Reynolds number, Pr is the Prandtl number, c is the speed of sound, and J is the transformation Jacobian. Pressure is related to the conservative flow variables $\hat{Q}$, through the equation of state for a perfect gas:

$$p = (\gamma - 1)\left[e - \frac{\rho}{2}(u^2 + v^2 + w^2) \right] \tag{2}$$

where ρ is the fluid density and e is total energy per unit of volume of the fluid.

For the inviscid case, the viscous flux $\widehat{G}^v$ is replaced by 0. For the viscous case, the viscosity coefficient μ in $\widehat{G}^v$ is computed as the sum of $\mu_l + \mu_t$ where the laminar viscosity μ_l is taken from the free-stream laminar viscosity, assumed to be constant for transonic flows, and the turbulent viscosity μ_t is evaluated by the Baldwin-Lomax model.[5]

NUMERICAL ALGORITHM

The space-discretized form of equation (1) can be written as

$$\partial_\tau \widehat{Q} = -\frac{\widehat{E}_{i+\frac{1}{2}} - \widehat{E}_{i-\frac{1}{2}}}{\Delta\xi} - \frac{\widehat{F}_{j+\frac{1}{2}} - \widehat{F}_{j-\frac{1}{2}}}{\Delta\eta} - \frac{\widehat{G}_{k+\frac{1}{2}} - \widehat{G}_{k-\frac{1}{2}}}{\Delta\zeta} + \frac{1}{Re}\frac{\widehat{G}^v_{k+\frac{1}{2}} - \widehat{G}^v_{k-\frac{1}{2}}}{\Delta\zeta} \tag{3}$$

where a second-order central-difference evaluation is applied to the viscous term.

The evaluation of the inviscid fluxes is based on the finite-volume cell-centered scheme. To be consistent with the finite-difference scheme in ENSAERO, the metrics are defined at each grid point where the flow variables are stored. The surface vector of cell-interface, which is necessary for the finite-volume formulation, can be obtained by averaging the metrics at the adjoining points. The free-stream preservation of this metric evaluation was shown in reference 6.

Streamwise Upwind Algorithm

The formula of the streamwise upwind algorithm on the fixed grid system ($\xi_t = \eta_t = \zeta_t = 0$) can be written in the cell-interface flux for the η-direction with a surface vector $\mathbf{S}$ normal to the ξ-ζ plane as follows:

$$\begin{aligned}\widehat{F}(Q_l, Q_r, \mathbf{S}_{j+\frac{1}{2}}) = &\frac{1}{2}\frac{|\nabla\eta|}{J}\Big(F_l\left[1 + \text{sign}(V_l)\cos^2\theta_l\right] + s_l\,\Delta^*(\rho q)_l\,\mathbf{e}_{sl}\cos^2\theta_l \\ &+ F_r\left[1 - \text{sign}(V_r)\cos^2\theta_r\right] - s_r\,\Delta^*(\rho q)_r\,\mathbf{e}_{sr}\cos^2\theta_r \\ &- [\,|V|\Delta Q + (c - |V|)(\frac{\Delta p}{c^2}\,\mathbf{e}_s + \rho\Delta V\,\mathbf{e}_d)\,]\sin^2\theta\Big)\end{aligned} \tag{4}$$

where $\Delta^*(\rho q) = \rho^* q^* - \rho q$ with local sonic values,

$$(q^*)^2 = \frac{2}{\gamma+1}(c^2 + \frac{\gamma-1}{2}q^2)$$

$$\rho^* = \rho\Big(\frac{(q^*)^2}{c^2}\Big)^{\frac{1}{\gamma-1}}$$

and where q is the velocity magnitude, $\mathbf{e}_s = (1, u, v, w, H)^T$, $\mathbf{e}_d = (0, k_x, k_y, k_z, k_x u + k_y v + k_z w)^T$, $\Delta\cdot = \cdot_r - \cdot_l$, $V = k_x u + k_y v + k_z w$, $k_x = \eta_x/|\nabla\eta|$, and so on. The basic scheme is first-order accurate with $l = j$ and $r = j+1$. The variables are averaged unless defined as a difference between left and right states. The switches $s_{l,r}$ and the rotation angle θ will be defined later. The $\cos^2\theta$ terms represent the projection on the coordinate axis from the streamwise flux vector splitting, and the $\sin^2\theta$ terms represent the projection on the crossflow plane for those terms that use the flux difference splitting. More details for the formulas are given in reference 4.

To extend equation (4) from a fixed-grid system to a moving-grid system, the flow velocity relative to the fixed grid, $\mathbf{q} = (u, v, w)$, is redefined as the flow velocity measured relative to the moving grid, $\tilde{\mathbf{q}} = (u - x_t, v - y_t, w - z_t)$. This is consistent with the modification of the definition of the contravariant velocity from a fixed-grid system,

$$\begin{aligned}\widehat{V}_{fixed} &= \eta_x u + \eta_y v + \eta_z w \\ &= \nabla\eta\cdot\mathbf{q}\end{aligned}$$

to a moving-grid system,

$$\begin{aligned}\widehat{V}_{moving} &= \eta_t + \eta_x u + \eta_y v + \eta_z w \\ &= \eta_x(u - x_t) + \eta_y(v - y_t) + \eta_z(w - z_t) \\ &= \nabla\eta\cdot\tilde{\mathbf{q}}\end{aligned}$$

where $\eta_t = -\eta_x x_t - \eta_y y_t - \eta_z z_t$. Thus, equation (4) can be rewritten for a moving-grid system by using the following redefined variables: $\tilde{q}^2 = (u - x_t)^2 + (v - y_t)^2 + (w - z_t)^2$ and $\tilde{V} = k_x(u - x_t) + k_y(v - y_t) + k_z(w - z_t)$. (Note that $\mathbf{e}_s$ and $\mathbf{e}_d$ remain unchanged because they originate in the eigenvectors of the Jacobian $\partial\widehat{F}/\partial\widehat{Q}$.)

Equation (4) is written in a vector form. If the formula is rewritten in component form, the present algorithm can be summarized with a surface vector $\mathbf{S}$ and a motion of its centroid, $\mathbf{x}_t = (x_t, y_t, z_t)$, as

$$\widehat{F}(Q_l, Q_r, \mathbf{S}_{j+\frac{1}{2}}, \mathbf{x}_{t_{j+\frac{1}{2}}}) = \frac{1}{2}\frac{|\nabla\eta|}{J}\{ F_l^+ + F_r^- \} \tag{5}$$

where

$$F_{l,r}^{\pm} = \begin{bmatrix} f_{l,r}^{\pm} \\ f_{l,r}^{\pm} u_{l,r} + k_x p_{l,r}^{\pm} \\ f_{l,r}^{\pm} v_{l,r} + k_y p_{l,r}^{\pm} \\ f_{l,r}^{\pm} w_{l,r} + k_z p_{l,r}^{\pm} \\ f_{l,r}^{\pm} H_{l,r} - k_t p_{l,r}^{\pm} + (|\tilde{V}_m|\Delta p - \tilde{V}_m \Delta_2)\sin^2\theta \end{bmatrix}$$

$$f_{l,r}^{\pm} = (\rho\tilde{V})_{l,r}\left[1 \pm \mathrm{sign}(\tilde{V}_{l,r})\cos^2\theta_{l,r}\right]$$
$$\pm s_{l,r}\,\Delta^*(\rho\tilde{q})_{l,r}\cos^2\theta_{l,r} \pm \rho_{l,r}|\tilde{V}_m|\sin^2\theta - \frac{1}{2}\Delta_1\sin^2\theta$$

$$p_{l,r}^{\pm} = p_{l,r}\left[1 \pm \mathrm{sign}(\tilde{V}_{l,r})\cos^2\theta_{l,r}\right] - \frac{1}{2}\Delta_2\sin^2\theta$$

where $\tilde{q}$ and $\tilde{V}$ are defined above, and where $\Delta_1 = (c_m - |\tilde{V}_m|)\frac{\Delta p}{c_m^2}$, $\Delta_2 = (c_m - |\tilde{V}_m|)\rho_m \Delta V$, and $k_t = -k_x x_t - k_y y_t - k_z z_t$. The averaged state (m) is defined for ρ, u, v, w, and H by the arithmetic average of the left (l) and right (r) states.

The switches s_l and s_r are defined in the manner of Godunov's method as follows. For $\tilde{V} \geq 0$,

$$\begin{aligned} s_l &= 1 - \epsilon_l\,\epsilon_m \\ s_r &= (1 - \epsilon_m)(1 - \epsilon_r) \end{aligned} \tag{6}$$

where

$$\epsilon_{l,m,r} = \frac{1}{2}\left[1 + \mathrm{sign}(M_{l,m,r}^2 - 1)\right]$$

and $M = \tilde{q}/c$.

A simple way to evaluate the rotation angle is to use $\cos\theta = \tilde{V}/\tilde{q}$. In supersonic flow fields, however, it is important to detect whether the velocity projected to the grid line is beyond the Mach cone. Thus, $\tilde{V}/\tilde{q}$ is replaced by $M \cdot \tilde{V}/\tilde{q} = \tilde{V}/c$. If $\tilde{V}/c$ becomes larger than one, $\cos\theta$ is set to one. To avoid expansion shocks, the rotation angle is determined by a mixture of averaged (m) and pointwise (l, r) values:

$$\cos^2\theta_{l,r} = \min\left[\ (1-\phi)\frac{\tilde{V}_m^2}{c_m^2} + \phi\frac{\tilde{V}_{l,r}^2}{c_{l,r}^2},\ 1\ \right] \tag{7}$$

The following relation is used here for evaluating $\phi \in [0, 1]$ because of the smoothness:

$$\phi = \max\left[\frac{2\gamma}{\gamma+1}\left\{1 - \frac{1}{2\gamma}[\gamma - 1 + (\gamma+1)\frac{p_2}{p_1}]\right\}, 0\right] \tag{8}$$

where p_1 and p_2 denote upstream and downstream pressures, respectively. The sine is determined by an arithmetic average of the cosines: $\sin^2\theta = 1 - \frac{1}{2}(\cos^2\theta_l + \cos^2\theta_r)$.

Higher-order schemes are constructed from a one-parameter family, κ, of interpolations of the primitive variables, ρ, u, v, w, and p. For example,

$$\begin{aligned} p_l &= \{1 + \frac{\psi_j}{4}[(1-\kappa)\nabla + (1+\kappa)\Delta]\}p_j \\ p_r &= \{1 - \frac{\psi_{j+1}}{4}[(1+\kappa)\nabla + (1-\kappa)\Delta]\}p_{j+1} \end{aligned} \tag{9}$$

where ∇ and Δ are backward and forward difference operators, respectively (ref. 7). For the third-order scheme, $\kappa = \frac{1}{3}$, Koren's differentiable limiter (ref. 8) is used here. The limiter ψ is calculated as

$$\psi_j = \frac{3\nabla p_j \Delta p_j + \epsilon}{2(\Delta p_j - \nabla p_j)^2 + 3\nabla p_j \Delta p_j + \epsilon} \tag{10}$$

where a small constant ϵ, $\epsilon = 10^{-6}$ typically, is added to prevent the division by zero. The same formulas are used for the other primitive variables.

LU-ADI Method

One of the time-marching methods for the present upwind scheme is the LU-ADI factorization method proposed by one of the present authors (ref. 6). The LU-ADI method is a compromise between ADI and LU factorization. Applied to equation (3), this method is written as,

$$\left(T_\xi L_A D_A U_A T_\xi^{-1}\right) \times \left(T_\eta L_B D_B U_B T_\eta^{-1}\right) \times \left(T_\zeta L_C D_C U_C T_\zeta^{-1}\right) \times \Delta\widehat{Q}^n = \Delta t R^n \tag{11}$$

where R represents the right-hand side of equation (3). The change of volume in time is neglected, assuming translational movements of the grids. On the left-hand side, the original ADI operator of the Beam-Warming method is rewritten using the diagonal form (ref. 9) and the first-order accurate Steger-Warming flux-vector splitting (ref. 10). For example, in the η-direction,

$$\begin{aligned} & I + \Delta t \delta_\eta \widehat{B} \\ &= T_\eta (I + \Delta t \nabla_\eta \widehat{D}_B^+ + \Delta t \Delta_\eta \widehat{D}_B^-) T_\eta^{-1} \\ &= T_\eta (I - \Delta t \widehat{D}_B^-|_j + \Delta t \nabla_\eta \widehat{D}_B^+)(I + \Delta t |\widehat{D}_B|_j)^{-1}(I + \Delta t \widehat{D}_B^+|_j + \Delta t \Delta_\eta \widehat{D}_B^-) T_\eta^{-1} \\ &= T_\eta L_B D_B U_B T_\eta^{-1} \end{aligned} \tag{12}$$

This factorization is the approximate LDU (lower-diagonal-upper) factorization. This is more stable than simple LU factorization since the diagonal element always has the absolute value of the eigenvalues.

Approximate Block ADI Method

The LU-ADI method described in the previous section is nonconservative in time owing to the diagonalization. To investigate the significance of this temporal nonconservativeness, an alternative approach is considered here. A time-conservative method can be constructed using a block-tridiagonal solver similar to the Beam-Warming method. Since true Jacobians of the numerical fluxes of the present upwind algorithm are expensive to compute, approximate Jacobians are used here.

To construct an implicit method for the present upwind algorithm, it is easier to start from the vector form (eq. (4)) rather than from the component form (eq. (5)). From equation (4), the first-order-accurate flux can be rewritten as

$$\begin{aligned}\widehat{F}_j^{\pm} = \frac{1}{2}\frac{|\nabla\eta|_{j\pm\frac{1}{2}}}{J_{j\pm\frac{1}{2}}}\Big\{ & F_j\left[1 \pm \mathrm{sign}(\tilde{V}_j)\cos^2\theta_j\right] \pm s_j\Delta^*(\rho\tilde{q})_j\cos^2\theta_j\mathbf{e}_{sj} \\ & \pm |\tilde{V}_{j\pm\frac{1}{2}}|\sin^2\theta\, Q_j \pm \frac{c_{j\pm\frac{1}{2}} - |\tilde{V}_{j\pm\frac{1}{2}}|}{c^2_{j\pm\frac{1}{2}}}\sin^2\theta\, \mathbf{e}_{sj\pm\frac{1}{2}}p_j \\ & \pm \rho_{j\pm\frac{1}{2}}(c_{j\pm\frac{1}{2}} - |\tilde{V}_{j\pm\frac{1}{2}}|)\sin^2\theta\, \mathbf{e}_{dj\pm\frac{1}{2}}V_j\Big\}\end{aligned} \tag{13}$$

To simplify the formula further, the $\mathbf{e}_{sj\pm\frac{1}{2}}$ term in the second line of the above formula is replaced by $\mathbf{e}_{sj}$. Then, the Jacobian $\partial\widehat{F}^{\pm}/\partial\widehat{Q}$ can be approximated as

$$\begin{aligned}\tilde{B}_j^{\pm} = \frac{J_j}{2}\frac{|\nabla\eta|_{j\pm\frac{1}{2}}}{J_{j\pm\frac{1}{2}}}\Big\{ & B_j[1 \pm \mathrm{sign}(\tilde{V}_j)\cos^2\theta_j] \\ & \pm [\, s_j\Delta^*(\rho\tilde{q})_j\cos^2\theta_j + \frac{c_{j\pm\frac{1}{2}} - |\tilde{V}_{j\pm\frac{1}{2}}|}{c^2_{j\pm\frac{1}{2}}}p_j\sin^2\theta]\; M_j \\ & \pm |\tilde{V}_{j\pm\frac{1}{2}}|\sin^2\theta\, I \pm \frac{\rho_{j\pm\frac{1}{2}}(c_{j\pm\frac{1}{2}} - |\tilde{V}_{j\pm\frac{1}{2}}|)\sin^2\theta}{\rho_j}N_{j\pm\frac{1}{2}}\Big\}\end{aligned} \tag{14}$$

where $B = \partial F/\partial Q$, I is the identity matrix,

$$M = \frac{1}{\rho}\frac{\partial\rho\mathbf{e}_s}{\partial Q} = \frac{1}{\rho}\begin{pmatrix} 1 & 0 & 0 & 0 & 0 \\ 0 & 1 & 0 & 0 & 0 \\ 0 & 0 & 1 & 0 & 0 \\ 0 & 0 & 0 & 1 & 0 \\ \frac{\gamma-1}{2}(u^2+v^2+w^2) & -(\gamma-1)u & -(\gamma-1)v & -(\gamma-1)w & \gamma \end{pmatrix}$$

$$N = \mathbf{e}_d\cdot(0, k_x, k_y, k_z, 0) = \begin{pmatrix} 0 & 0 & 0 & 0 & 0 \\ 0 & k_x^2 & k_xk_y & k_xk_z & 0 \\ 0 & k_yk_x & k_y^2 & k_yk_z & 0 \\ 0 & k_zk_x & k_zk_y & k_z^2 & 0 \\ 0 & V^fk_x & V^fk_y & V^fk_z & 0 \end{pmatrix}$$

and where $V^f = k_x u + k_y v + k_z w$. The switches and the angles are evaluated identically to the explicit formulas. Similar to the results discussed in reference 11, this approach yields a method that is less stable than the LU-ADI method.

Neglecting the viscous terms, the approximate block ADI method can be written as

$$\left(I + \Delta t \frac{\tilde{A}^-_{i+1} + \tilde{A}^+_i - \tilde{A}^-_i - \tilde{A}^+_{i-1}}{\Delta \xi}\right)$$
$$\times \left(I + \Delta t \frac{\tilde{B}^-_{j+1} + \tilde{B}^+_j - \tilde{B}^-_j - \tilde{B}^+_{j-1}}{\Delta \eta}\right) \qquad (15)$$
$$\times \left(I + \Delta t \frac{\tilde{C}^-_{k+1} + \tilde{C}^+_k - \tilde{C}^-_k - \tilde{C}^+_{k-1}}{\Delta \zeta}\right) \Delta \hat{Q}^n = \Delta t R^n$$

In contrast to the LU-ADI method, the resulting method is conservative. However, both methods are first-order accurate in time. This method requires twice as much CPU time as the LU-ADI method.

RESULTS

Time-accuracy is an essential requirement for aeroelastic computations. Numerical schemes used for flow calculations in aeroelasticity must guarantee the correct calculation of the amplitude and phase of unsteady pressures. In order to verify the time-accuracy of the present code, unsteady flows over a rectangular wing undergoing a prescribed oscillatory motion are computed.

The test cases consider inviscid and viscous unsteady flows over a rectangular wing with a NACA 64A010 airfoil section and an aspect ratio of 4. Steady and unsteady measured data from wind-tunnel tests of this wing are given in reference 12. The unsteady data are given for the case in which the rigid wing is oscillating in the pitching mode, $\alpha(t) = \alpha_m - \alpha_0 \sin(\omega t)$, about an axis at $x/c_r = 0.5$, where c_r is the reference chord length, and ω is the pitching frequency in radians per second. The inviscid flow is computed at $M_\infty = 0.8$ with a mean angle of attack $\alpha_m = 0°$, pitch amplitude $\alpha_0 = 1°$, and reduced frequency k= 0.27 (k= $\omega c_r / U_\infty$). In addition, for the viscous flow, the Reynolds number based on the wing chord is $Re = 2 \times 10^6$. The Baldwin-Lomax model (ref. 5) is used to compute the turbulent eddy-viscosity coefficient for this case.

The C-H-type grid system is used for the present computations. The ξ, η, and ζ coordinates represent the chordwise, spanwise, and normal (to the wing surface) directions, respectively. For the inviscid computations, coarse and fine grids are used. The coarse grid contains $91 \times 25 \times 25$ points in the ξ, η, and ζ-coordinate directions, respectively, and the fine grid contains $151 \times 25 \times 34$ points. These grids have a minimum spacing normal to the wing of $0.01 c_r$. The viscous grid also contains $151 \times 25 \times 34$ points and has the minimum spacing normal to the wing of $0.00005 c_r$. This yields a value of $y^+ \leq 6$ at the first grid point above the wing surface. The grids are generated algebraically.

Unsteady computations are started from the corresponding steady-state solution. The stability of unsteady computations is verified by increasing the numbers of time-steps per cycle until no change is

noticed in the unsteady results. The convergence of the unsteady computations to a periodic flow is verified by comparing the results between cycles. For all cases considered here, the results for the third cycle give pressure profiles that are identical to those of the second-cycle results. Thus, the numerical transient is confirmed to disappear within two cycles.

The present upwind results are also compared with the results obtained by using the existing CD method. Reference 13 discusses the CD results obtained from the same test case. The CD method uses the diagonal inversions of the Beam-Warming method (ref. 9), and thus it is first-order accurate but non-conservative in time. Its artificial dissipation model consists of second- and fourth-order dissipation terms controlled by the amount of the second-difference of pressure.

Inviscid Solutions

First, the inviscid coarse-grid ($91 \times 25 \times 25$ points) solutions are presented. Figure 1 compares the computed and measured unsteady, upper-surface pressure coefficients for the real and imaginary parts of the first Fourier component. Pressure coefficients are shown for various span locations. The computations were done by using the upwind algorithm with the LU-ADI method (UP-LU). The solid, dashed, and dotted lines in the figure indicate the results obtained using 1440, 720, and 360 time-steps per cycle of oscillation (steps/cycle), respectively. (The time-steps per cycle rate of 1440 corresponds to $\Delta t \simeq 0.02$.) The solution profiles obtained using 1800 steps/cycle coincided with those using 1440 steps/cycle. Thus, the unsteady pressure profiles converged with respect to time-step sizes at 1440 steps/cycle. In addition, because the differences between the results with 720 and 1440 steps/cycle are not critical when making comparisons with experimental data, the computation with 720 steps/cycle is acceptable for numerical efficiency.

Figure 2 shows the analogous CD results. In this case, the second- and fourth-order dissipation coefficients are fixed at 0.25 and 0.01, respectively (denoted as CD(0.01)). These coefficients are the values that were used in references 1, 2, 9 and 13. The CD results show less dependence on time-step size than do the UP-LU results, although the profiles are smeared out at the large-gradient region near the shock wave and leading-edge regions. In order to check the dependence of the CD method on the amount of numerical dissipation, computations were tried with half the amount of dissipation coefficients (0.125, 0.005). At 360 steps/cycle, the computation became unstable with these coefficients. At 720 and 1440 steps/cycle, the computations were stable, but the resulting unsteady pressure profiles were still smeared out.

Figure 3 shows the results using the approximate block ADI method applied to the present upwind algorithm (UP-BL). The UP-BL method was not stable for computations using 360 and 720 steps/cycle, and thus the computations were done using 1080, 2160, and 3600 steps/cycle. The solution profiles obtained with 3600 steps/cycle finally showed good agreement with the UP-LU result converged at 1440 steps/cycle.

Figure 4 compares the three methods, UP-LU, UP-BL, and CD(0.01), fixing the number of time-steps per cycle at 1440. Both UP-LU and UP-BL results give similar profiles at the shock motion, although the UP-LU method is nonconservative in time. Both upwind methods give better agreement with the experimental data in the region of the shock motion than the CD method.

These results indicate that the temporally nonconservative LU-ADI method is valid for unsteady computations, even with moving shock waves, when the number of time-steps per cycle is large (i.e., small Δt). In the present case, any number of time-steps per cycle greater than 720 will give a reasonable result. The CD method also uses the temporally nonconservative diagonal form. However, the CD result differs from both the upwind results. This indicates that the solution depends on the numerical dissipation more than on the time-conservative properties of the methods.

The coarse-grid computations took 18.0, 19.5 and 42.3 μsec per grid point per time-step for the CD, UP-LU, and UP-BL methods, respectively, on a CRAY-YMP computer using a single processor. Although the UP-BL method is the most expensive, its accuracy does not appear to compensate for the computational inefficiency. Thus, the UP-BL method will be dropped in the following computations.

Next, the inviscid computations were done on a finer ($151 \times 25 \times 34$ points) grid. Since detailed comparisons with respect to time-step sizes are done on the coarse grid, the results are highlighted in the comparison of the UP-LU and CD solutions, as shown in figure 5. Both computations use 720 steps/cycle, as suggested in the coarse-grid case, because the time-step requirement for the fine-grid case is expected to be the same as that for the coarse-grid case (note that both grids have the same minimum spacing size normal to the wing). The fine-grid computations took 15.5 and 16.8 μsec per grid point per time-step for the CD and UP-LU methods, respectively.

For the CD method shown in figure 5, the two sets of the second- and fourth-order dissipation coefficients (0.25, 0.01) and (0.125, 0.005), indicated as CD(0.01) and CD(0.005), respectively, are used to illustrate the effect of the artificial dissipation. The CD solutions approach the UP-LU solution at 50% and 77% semispan locations as the dissipation coefficients are reduced. However, the shock profile becomes too steep and the post-shock oscillation in the plot becomes deep at the root section. Further reduction of the dissipation coefficients (to 0.0625, 0.0025) made the computation unstable. Compared with the coarse-grid solution shown in figure 4, the CD solutions also tend to converge to the UP-LU solutions because of the grid refinement. Therefore, the UP-LU method is confirmed to give a less dissipative and thus more accurate solution than the CD method.

Viscous Solutions

To demonstrate the capability of the UP-LU method for viscous computations, the same case has been computed with the viscous terms. The viscous grid has the same number of grid points as the inviscid fine grid, but with a smaller spacing in the ζ-direction normal to the wing. Because of the stiffness caused by the clustered viscous grids, time-step sizes used in the CD computations are usually determined by stability considerations rather than by time-accuracy (ref. 13). Two time-steps/cycle rates were chosen to demonstrate the robustness and accuracy of the UP-LU method. The results are again highlighted in the comparison of the UP-LU and CD solutions at specified time-step sizes.

Figure 6 compares the viscous solutions using the UP-LU, CD(0.01), and CD(0.02) methods with 720 steps/cycle. This number of time-steps per cycle is too small to obtain accurate and stable results for the CD method, a finding also reported in reference 13. The numerical instabilities in the CD results are

shown by oscillations in the pressure profiles of CD(0.01). However, the UP-LU result shows that the UP-LU method relaxes this stability requirement. Thus, time-step sizes for the UP-LU method are not limited by stability considerations even for the viscous case.

Figure 7 shows the corresponding results with 1440 steps/cycle. This is the time-step rate suggested in reference 13. Here, the CD(0.01) solution becomes stable and agrees reasonably well with the experimental data. To check whether the amount of dissipation is reasonable, the dissipation coefficients were reduced by half, as was done for the inviscid case, but the CD(0.005) computation diverged for the viscous case. In figure 7, and analogous to the inviscid results shown in figure 5, the CD solutions approach the UP-LU solution as the dissipation coefficients are reduced. Again the UP-LU method is confirmed to give a less-dissipative and thus more accurate solution than the CD method. The viscous solutions in figure 7 are similar to the inviscid solutions in shown in figure 5 because the experimental flow field does not contain strong viscous effect (ref. 12).

These results also indicate that the CD method is sensitive to both time-step size and to the amount of artificial dissipation added. Therefore, users of the CD method are required to find an adequate combination of time-step size and dissipation coefficients on a case-by-case basis. In contrast, the UP-LU method is robust, and users do not have to find any dissipation coefficient.

For the viscous case, the UP-LU computation requires 18.9 μsec per grid point per time step at a speed of 141 MFLOPS on a CRAY-YMP computer using a single processor, and the CD computation requires 17.1 μsec at a speed of 132 MFLOPS. There is 11% increase of CPU time when the upwind option of the code is used.

CONCLUSIONS

A new streamwise upwind algorithm has been derived to compute unsteady flow fields with a moving grid system. The temporally nonconservative lower-upper-factored, alternating-direction-implicit (LU-ADI) method has been applied to compute flow over an oscillating wing at a transonic Mach number. A comparison of the temporally nonconservative method with a time-conservative version of the upwind scheme indicates that the solutions are insensitive to the time-conservativeness of the implicit solvers when practical time-step sizes are used. The temporally nonconservative upwind method was found to be more stable and twice as efficient as the time-conservative block ADI scheme, even though the block ADI scheme employed an approximate form of the Jacobians. Comparisons have been made between results obtained with both upwind schemes, with experimental measurements, and with computed results obtained using the existing central-difference method.

Comparisons with experimental data show that the upwind algorithm predicts the shock motion better than the central-difference (CD) method. The CD solutions are also found to be sensitive to the amount of numerical dissipation, and as a result, the dissipation coefficients must be specified case by case. In comparison, the present upwind method does not require a dissipation coefficient. Thus, the method that combines the streamwise upwind and LU-ADI methods is proposed for practical computations. This new upwind method is incorporated in the aeroelastic code ENSAERO. The new upwind option of the code allows larger time-steps and thus is more efficient, even though it requires slightly more computational time per time-step than the CD option.

REFERENCES

1. Guruswamy, G. P.: Time-Accurate Unsteady Aerodynamic and Aeroelastic Calculations of Wings Using Euler Equations. AIAA Paper 88-2281, 1988.

2. Guruswamy, G. P.: Vortical Flow Computations on Swept Flexible Wings Using Navier-Stokes Equations. AIAA Paper 89-1183, 1989.

3. Goorjian, P. M.: A New Algorithm for the Navier-Stokes Equations Applied to Transonic Flows over Wings. AIAA Paper 87-1121-CP, 1987.

4. Obayashi, S.; and Goorjian, P. M.: Improvements and Applications of a Streamwise Upwind Algorithm. AIAA Paper 89-1957-CP, 1989.

5. Baldwin, B. S.; and Lomax, H.: Thin Layer Approximation and Algebraic Model for Separated Turbulent Flows. AIAA Paper 78-257, 1978.

6. Obayashi, S.: Numerical Simulation of Underexpanded Plumes Using Upwind Algorithms. AIAA Paper 88-4360-CP, 1988.

7. Anderson, W. K.; Thomas, J. L.; and van Leer, B.: A Comparison of Finite Volume Flux Vector Splittings for the Euler Equations. AIAA Paper 85-0122, 1985.

8. Koren B.: Upwind Schemes, Multigrid and Defect Correction for the Steady Navier-Stokes Equations. Proceedings of 11th International Conference on Numerical Methods in Fluid Dynamics, June, 1988.

9. Pulliam, T. H.; and Steger, J. L.: Recent Improvements in Efficiency, Accuracy, and Convergence for Implicit Approximate Factorization Algorithms. AIAA Paper 85-360, 1985.

10. Steger, J. L.; and Warming, R. F.: Flux Vector Splitting of the Inviscid Gas-Dynamic Equations with Application to Finite-Difference Methods. J. Comp. Phys., vol. 40, 1981, pp. 263-293.

11. Liou, M-S.; and van Leer, B.: Choice of Implicit and Explicit Operators for the Upwind Differencing Method. AIAA Paper 88-0624, 1988.

12. Mabey, D. G.; Welsh, B. L.; and Pyne, C. R.: A Summary of Measurements of Steady and Oscillatory Pressures on a Rectangular Wing. Aeronaut. J. R. Aeronaut. Soc., Jan. 1988.

13. Chaderjian, N. M.; and Guruswamy, G. P.: Unsteady Transonic Navier-Stokes Computations for an Oscillating Wing Using Single and Multiple Zones. AIAA Paper 90-0313, 1990.

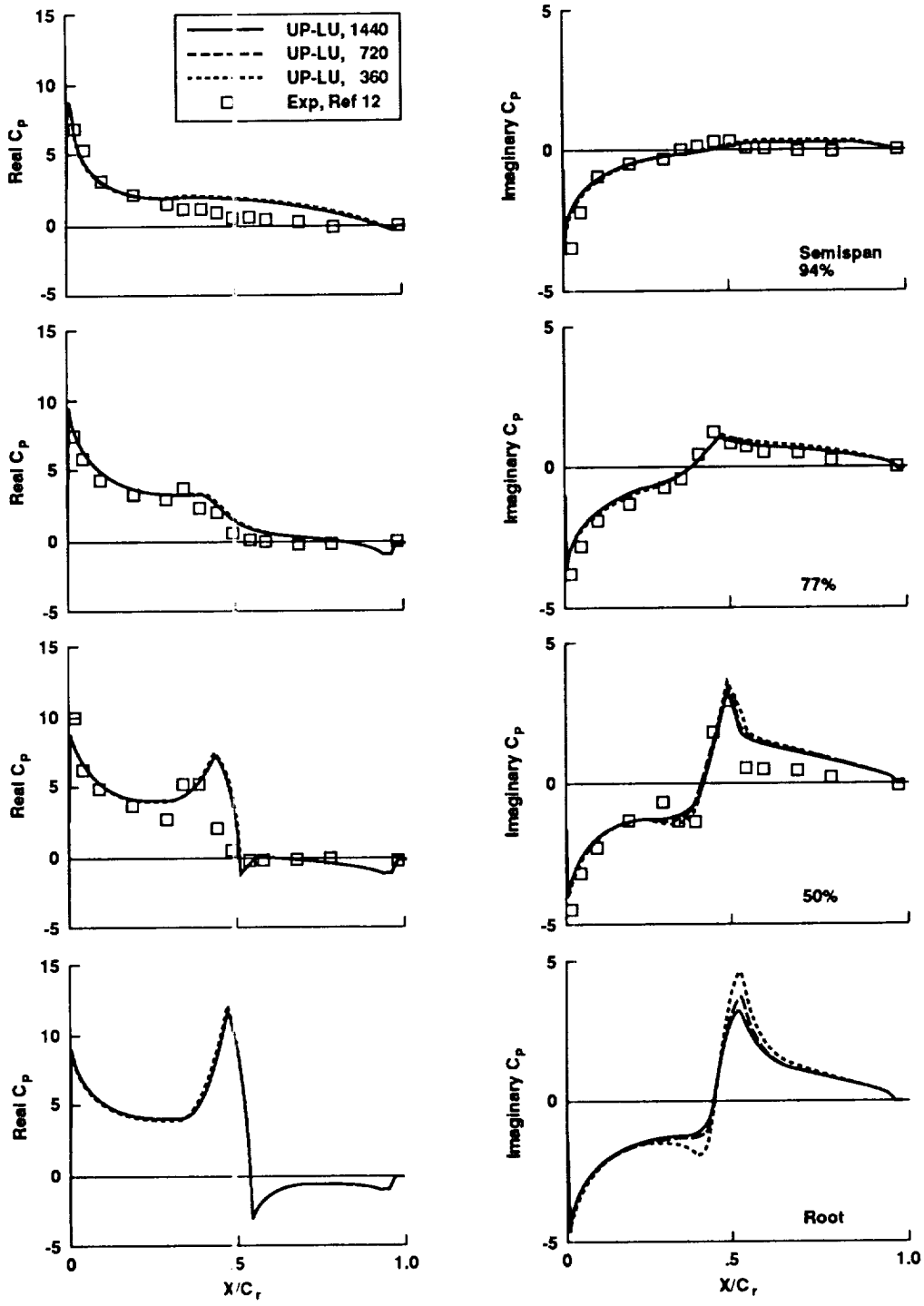

Figure 1. Effect of time-step sizes on inviscid upper-surface unsteady pressures for the rectangular wing computed by using the upwind LU-ADI method: 91 × 25 × 25 grid, $M_\infty = 0.8$, $\alpha_m = 0°$, k = 0.27, and $\alpha_0 = 1°$.

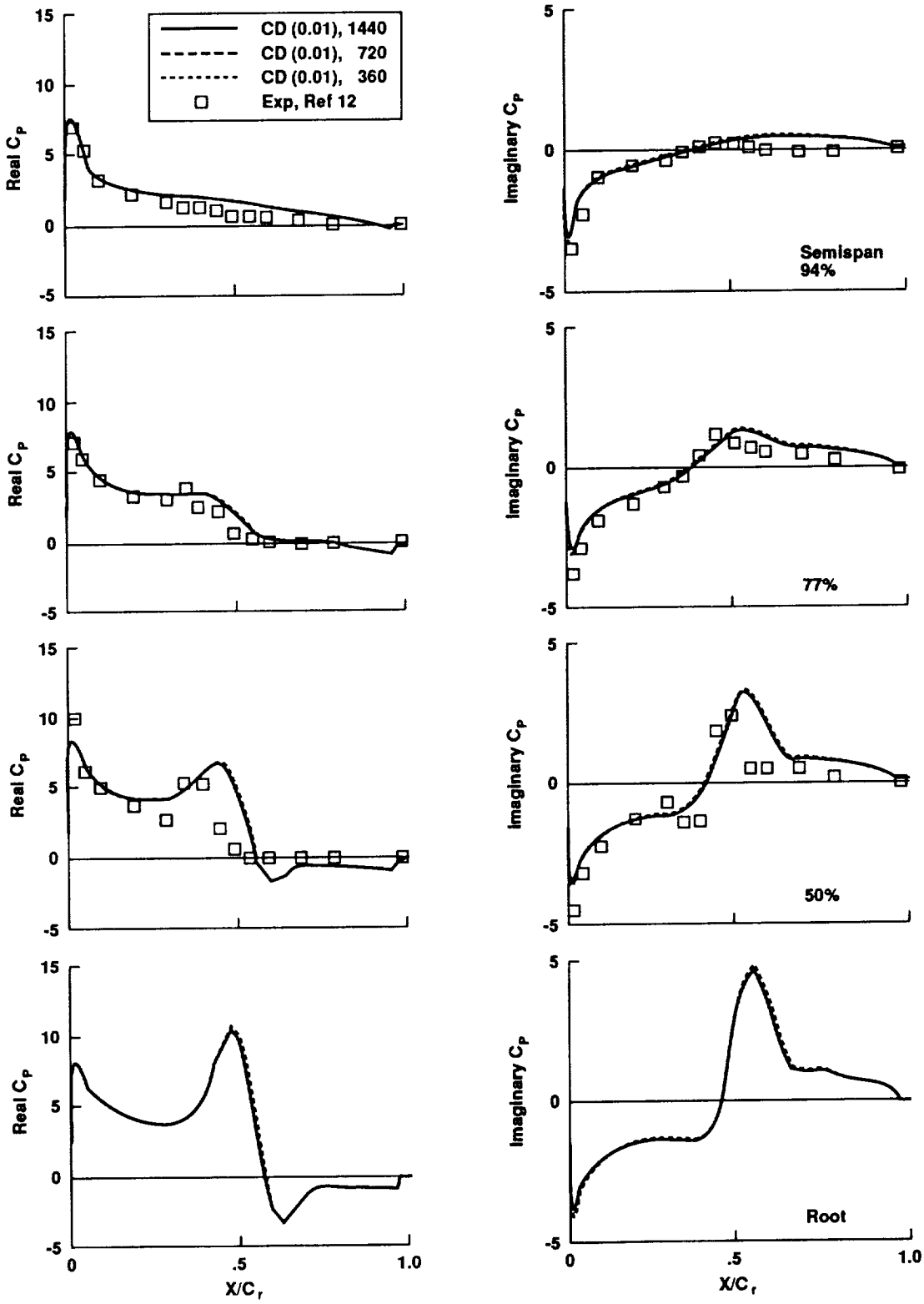

Figure 2. Effect of time-step sizes on inviscid upper-surface unsteady pressures for the rectangular wing computed by using the central-difference method: 91 × 25 × 25 grid, $M_\infty = 0.8$, $\alpha_m = 0°$, k = 0.27, and $\alpha_0 = 1°$.

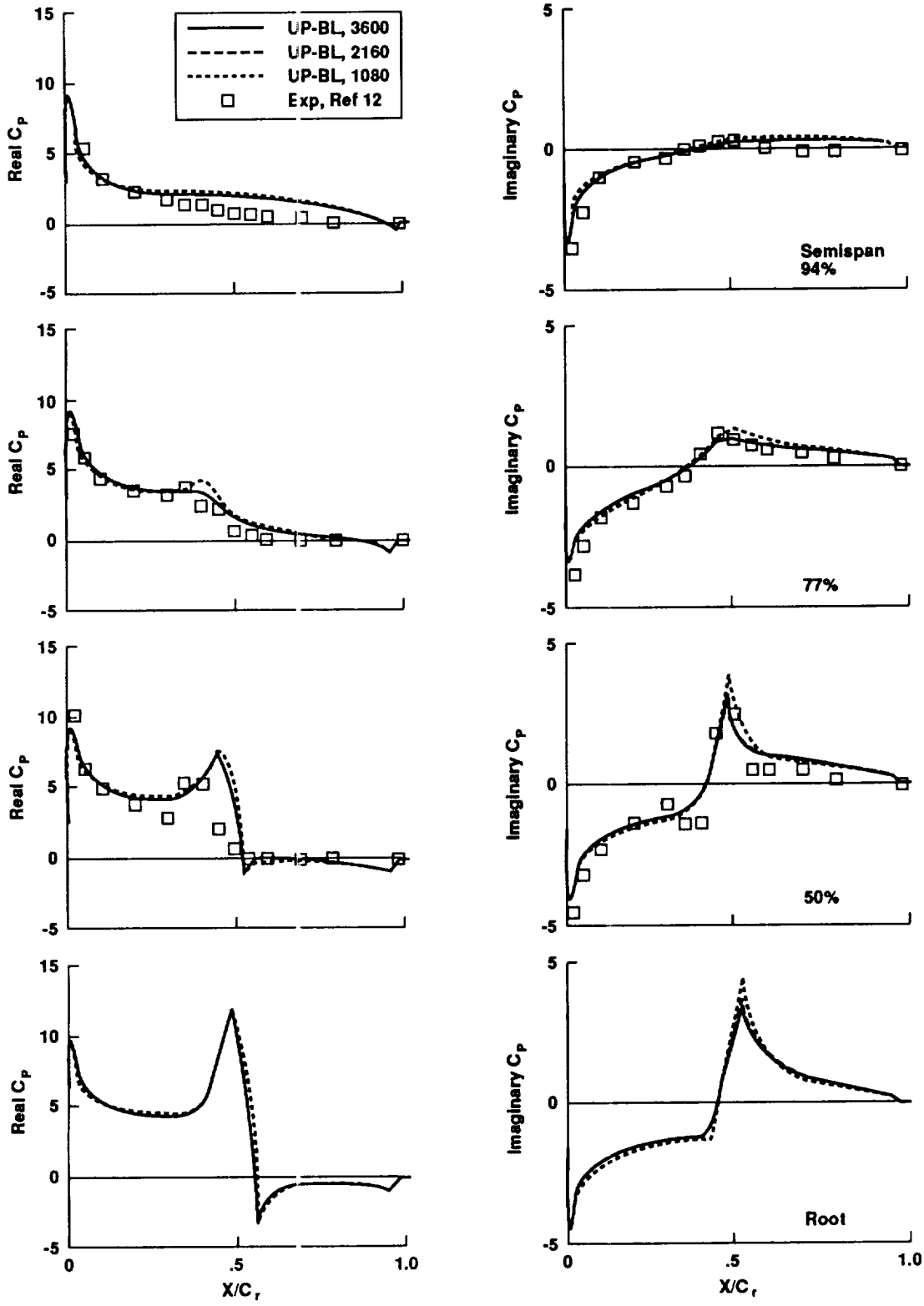

Figure 3. Effect of time-step sizes on inviscid upper-surface unsteady pressures for the rectangular wing computed by using the upwind block ADI method: 91 × 25 × 25 grid, $M_\infty = 0.8$, $\alpha_m = 0°$, k = 0.27, and $\alpha_0 = 1°$.

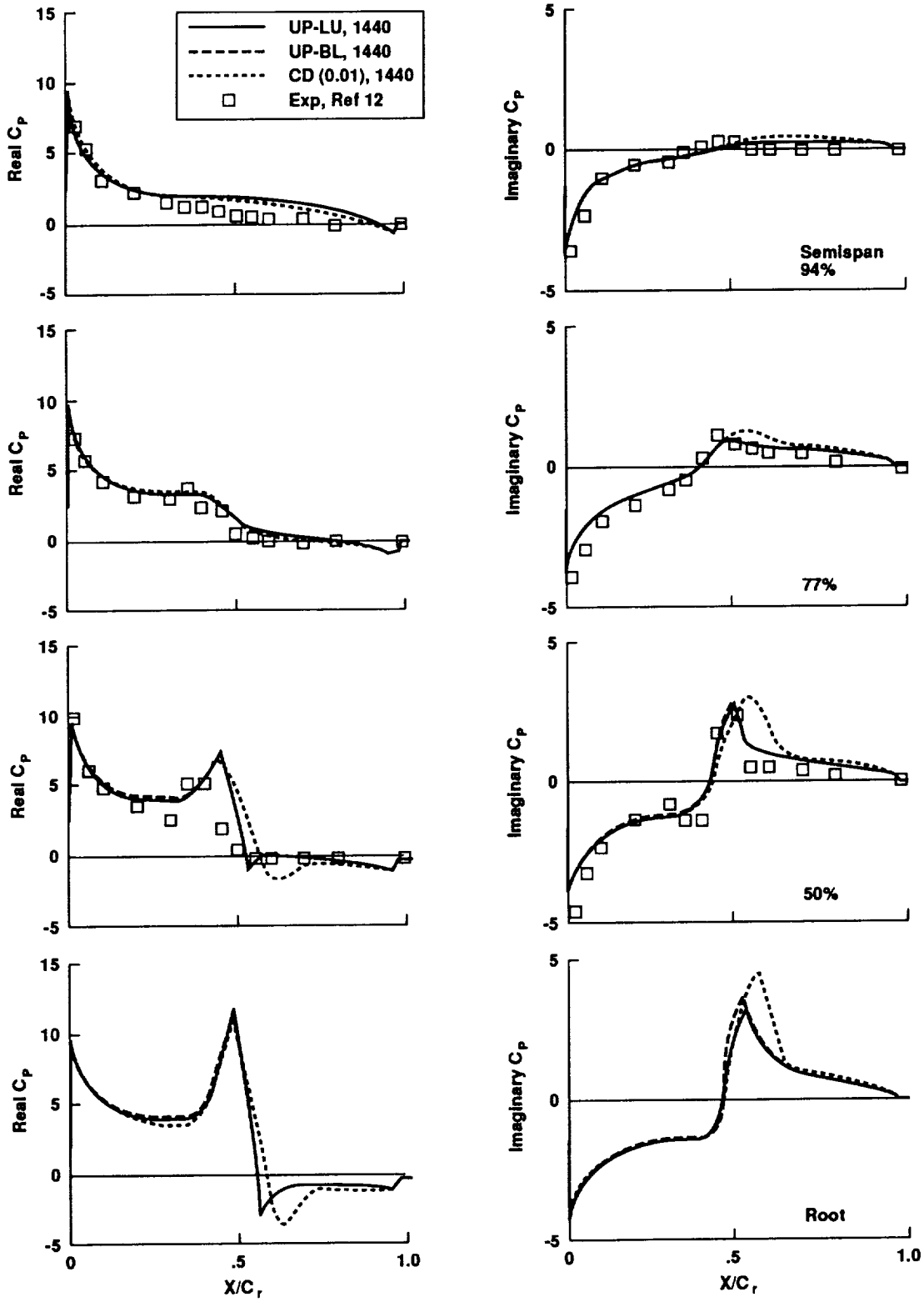

Figure 4. Comparison of inviscid upper-surface unsteady pressures computed by using the upwind LU-ADI, upwind block ADI, and central-difference methods with 1440 time-steps/cycle: 91 × 25 × 25 grid, $M_\infty = 0.8$, $\alpha_m = 0°$, k = 0.27, and $\alpha_0 = 1°$.

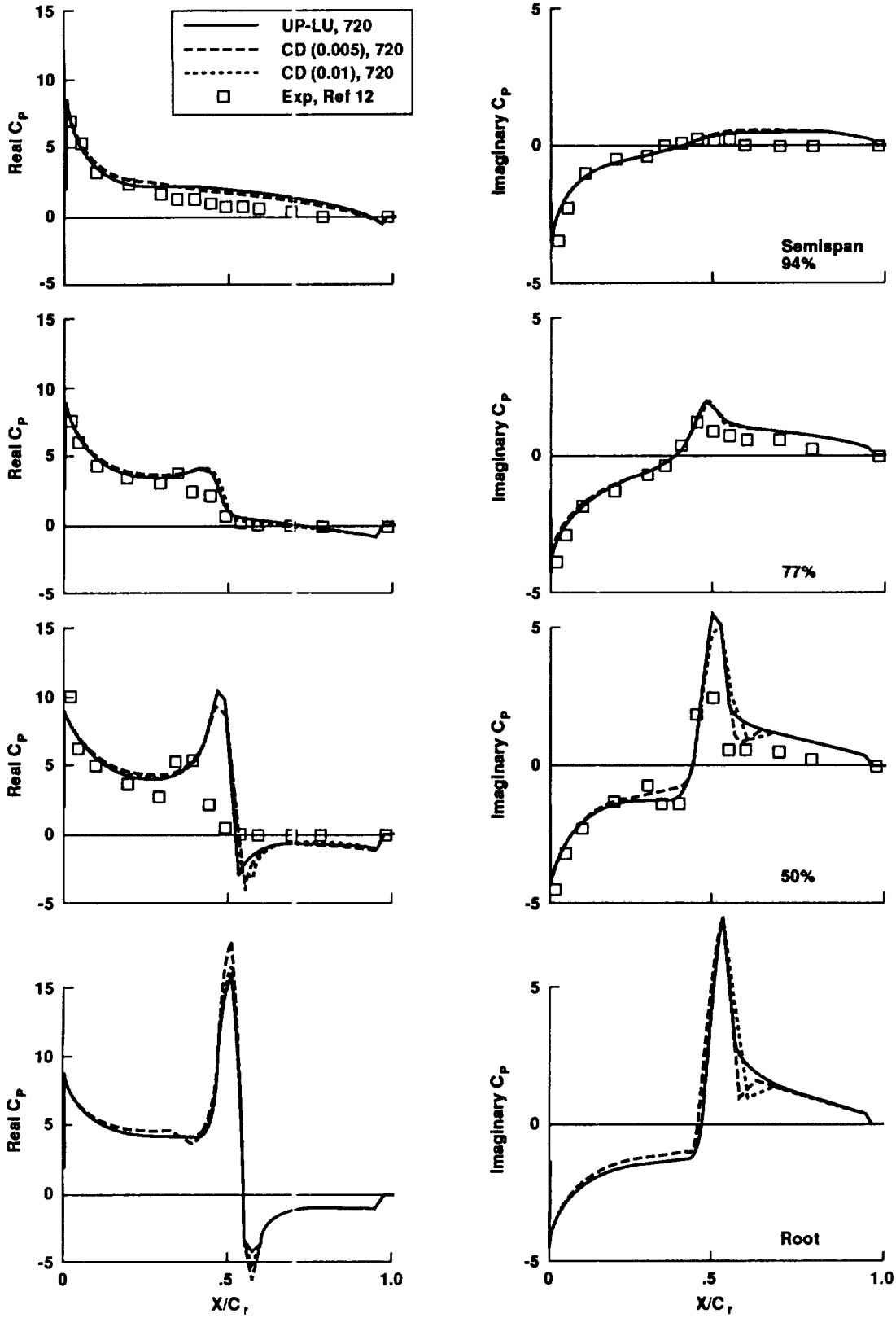

Figure 5. Comparison of inviscid upper-surface unsteady pressures computed by using the upwind LU-ADI method and the central-difference method with two sets of dissipation coefficients: 151 × 25 × 34 grid, $M_\infty = 0.8$, $\alpha_m = 0°$, k = 0.27, and $\alpha_0 = 1°$.

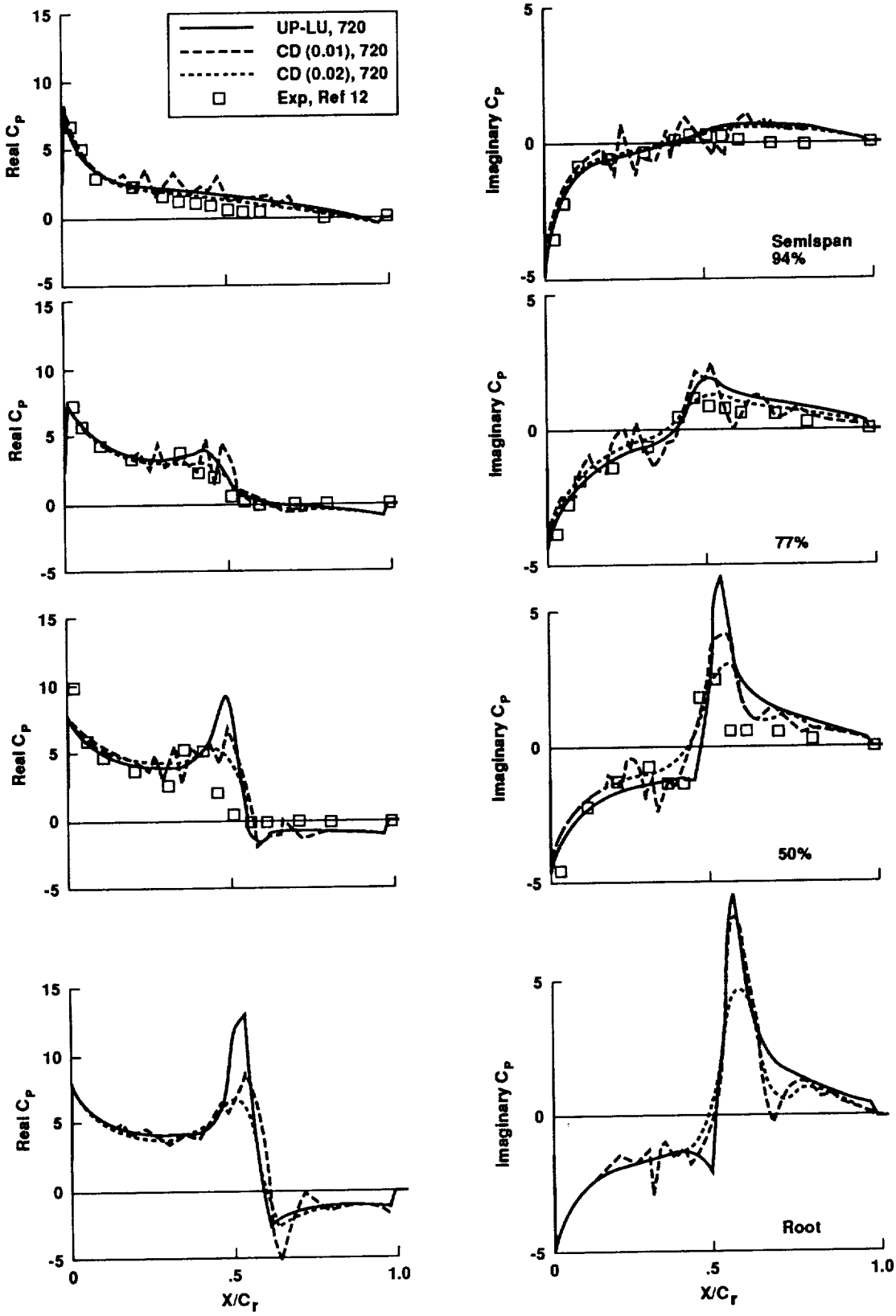

Figure 6. Comparison of viscous upper-surface unsteady pressures computed by using 720 time-steps/cycle: 151 × 25 × 34 grid, $Re = 2 \times 10^6$, $M_\infty = 0.8$, $\alpha_m = 0°$, k = 0.27, and $\alpha_0 = 1°$.

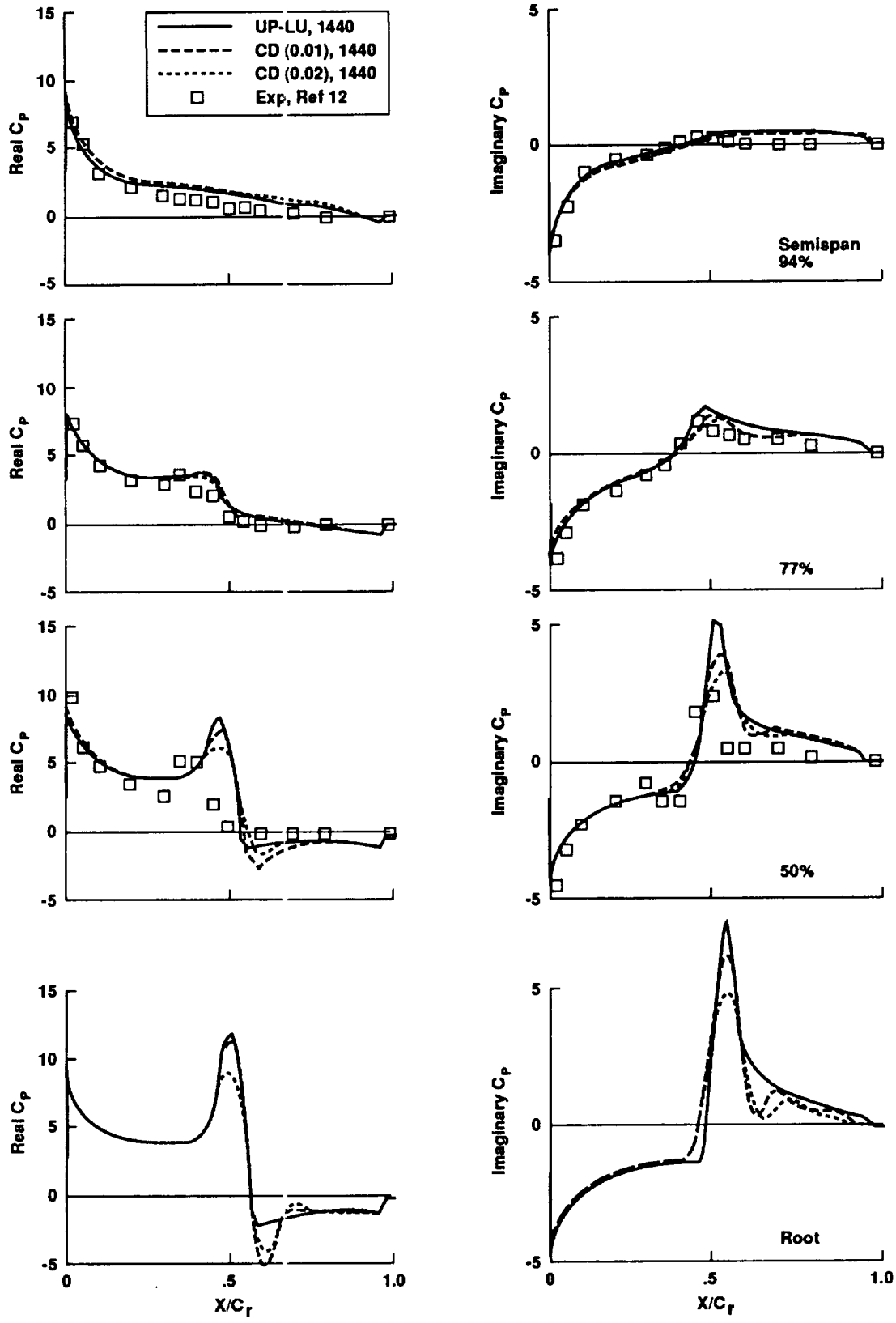

Figure 7. Comparison of viscous upper-surface unsteady pressures computed by using 1440 time-steps/cycle: 151 × 25 × 34 grid, $Re = 2 \times 10^6$, $M_\infty = 0.8$, $\alpha_m = 0°$, k = 0.27, and $\alpha_0 = 1°$.

NASA
National Aeronautics and Space Administration

Report Documentation Page

1. Report No.	2. Government Accession No.	3. Recipient's Catalog No.
NASA TM-102800		

4. Title and Subtitle	5. Report Date
Extension of a Streamwise Upwind Algorithm to a Moving Grid System	April 1990
	6. Performing Organization Code

7. Author(s)	8. Performing Organization Report No.
Shigeru Obayashi,* Peter M. Goorjian, and Guru P. Guruswamy	A-90101
	10. Work Unit No. 505-60

9. Performing Organization Name and Address	11. Contract or Grant No.
Ames Research Center Moffett Field, CA 94035-1000	
	13. Type of Report and Period Covered Technical Memorandum
12. Sponsoring Agency Name and Address	14. Sponsoring Agency Code
National Aeronautics and Space Administration Washington, DC 20546-0001	

15. Supplementary Notes

*MCAT Institute, San Jose, California

Point of Contact: Shigeru Obayashi, Ames Research Center, MS 258-1
Moffett Field, CA 94035-1000 (415) 604-4982 or FTS 464-4982

16. Abstract

A new streamwise upwind algorithm has been derived to compute unsteady flow fields with the use of a moving-grid system. The temporally nonconservative LU-ADI (lower-upper-factored, alternating-direction-implicit) method has been applied for time-marching computations. A comparison of the temporally nonconservative method with a time-conservative implicit upwind method indicates that the solutions are insensitive to the conservative properties of the implicit solvers when practical time-steps are used. Using this new method, computations have been made for an oscillating wing at a transonic Mach number. The computed results confirm that the present upwind scheme captures the shock motion better than the central-difference scheme based on the Beam-Warming algorithm. The new upwind option of the code allows larger time-steps and thus is more efficient, even though it requires slightly more computational time per time-step than the central-difference option.

17. Key Words (Suggested by Author(s))	18. Distribution Statement
Unsteady flows Upwind algorithm Navier-Stokes computations Moving grids	Unclassified-Unlimited Subject Category - 02

19. Security Classif. (of this report)	20. Security Classif. (of this page)	21. No. of Pages	22. Price
Unclassified	Unclassified	22	A02

NASA FORM 1626 OCT 86

For sale by the National Technical Information Service, Springfield, Virginia 22161